Eurographics Workshop on Visual Computing for Biology and Medicine (2019)
B. Kozlíková, L. Linsen, and P.-P. Vázquez (Editors)

Using Position-Based Dynamics for Simulating the Mitral Valve in a Decision Support System

Lars Walczak[1,2], Joachim Georgii[1], Lennart Tautz[1,2], Mathias Neugebauer[1], Isaac Wamala[3], Simon Sündermann[2,3], Volkmar Falk[2,3] and Anja Hennemuth[1,2]

Lars Walczak
lars.walczak@mevis.fraunhofer.de
[1] Fraunhofer MEVIS, Bremen, Germany
[2] Charité - Universitätsmedizin Berlin, Berlin, Germany
[3] German Heart Institute Berlin - DHZB, Berlin, Germany

Abstract

In mitral valve interventions, surgeons have to select an optimal combination of techniques for every patient. Especially less experienced physicians would benefit from decision support for this process. To support the visual analysis of the patient-specific valvular dynamics and an in-silico pre-intervention simulation of different therapy options, a real-time simulation of the mitral valve is needed, especially for the use in a time-constrained clinical environment. We develop a simplified model of the mitral valve and propose a novel approach to simulate the mitral valve with position-based dynamics. As input, a mesh representation of the open-state mitral valve, two polygons representing the open and closed annulus states, simplified chordae tendineae, and a set of forces for approximating the surrounding blood are required. The mitral valve model can be deformed to simulate the closing and opening as well as incorporate changes caused by virtual interventions in the simulation. For evaluation, ten mitral valves were reconstructed from transesophageal echocardiogram sequences of patients with normal and abnormal physiology. Experts in cardiac surgery annotated anatomical landmarks for valve reconstruction. The simulation results for closing the valve were qualitatively compared to the anatomy depicted in the image sequences and, if present, the reproduction of a prolapse was verified. In addition, two virtual interventions (annuloplasty and clipping) were performed for one case and provided new insights about changes in valve closure and orifice area after modification. Each simulation ran at interactive frame rates. Our approach enables an efficient simulation of the mitral valve with normal and abnormal valve closing behavior as well as virtual interventions. The simulation results showed good agreements with the image data in general and reproduced valve closure in all cases. In three cases, prolapse was not or not correctly reproduced. Further research is needed to parameterize the model in pathologic cases.

CCS Concepts

• ***Applied computing*** → ***Life and medical sciences; Health informatics;***

1. Introduction

The mitral valve (MV) is part of the left heart (LH) and is positioned between the left atrium (LA) and the left ventricle (LV). Two leaflets form the valve, which is attached to the mitral annulus (MA) and the chordae tendineae (CT). The chordae tendineae are connected to the papillary muscles (PM), which extend from the wall of the heart into the ventricle. The valve is open during ventricle filling and is closed during the contraction phase. In closed state, blood flow back to the atrium is normally prevented by combined parachute-like action of the leaflets, chordae tendineae, and papillary muscles (cf. Fig. 1(a)-1(b)).

In Germany, mitral valve regurgitation (MR) is the second most common heart valve disease with an increasing incidence [KSH18]. Patients with MR exhibit defects in the leaflets or chordae tendineae, but numerous other pathological anatomical alterations are possible as well. This results in an incomplete closure or prolapse into the atrium (cf. Fig. 1(c)-1(d)). In turn, this leads to blood flowing back into the atrium during heart contraction (cf. Fig. 1(a)). This impairs heart function and increases the volume-load on the LA. Several therapy options exist to treat MR. The range spans from reconstruction using different catheter-based or surgical techniques to complete valve replacement. More than 12,300 MV procedures were performed in Germany in 2017 [BML*18]. Surgical reconstruction is the gold standard therapy for MR with very good long-term results [SBF*08, SSB*14]. Nevertheless, the success rate of MV procedures should be improved. Basis for therapy decisions is the visual as well as the quantitative assessment of the valve anatomy and function through imaging. The gold standard diagnostic tool is echocardiography. Trans-

DOI: 10.2312/vcbm.20191242

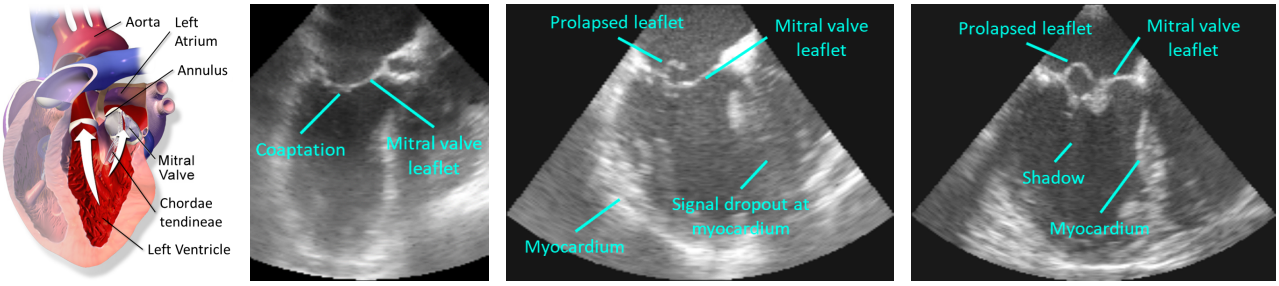

(a) (b) (c) (d)

Figure 1: ***(a)*** *Illustration of heart anatomy with MR (image adapted from [Bla14]).* ***(b)-(d)*** *Images showing the heart in long axis view.* ***(b)*** *normal valve,* ***(c)-(d)*** *abnormal (prolapsing) leaflets. A disadvantage of TEE acquisitions are shadowing and signal dropout artifacts. In the open state, the leaflets can also be positioned very close to the myocardium, while in the closed state, the coaptation (zone where the leaflets meet) can be difficult to assess. Anatomical structures, landmarks, and acquisition artifacts (shadowing, signal dropout at myocardium) are highlighted.*

esophageal echocardiograms (TEE, cf. Fig. 1(b)-1(d)) are acquired before, during, and after a minimal-invasive or catheter-based mitral valve intervention. Although TEE exhibits artifacts, such as signal dropout (cf. Fig.1(c)) or shadowing effects (cf. Fig.1(d)), the images are used for planning, guiding, and success rating. A relatively high temporal and spatial resolution of the 3D+t image data sets enables measurements and visualization of relevant structures for intervention planning in different cardiac phases. However, this is only a depiction of the anatomy at recording time. After the imaging-based preparation, the further planning of the intervention has to be discussed and gone through in the surgeons' minds. At this stage, more subjective aspects affect the preparation, and the choice of therapy is not only based on guidelines but also on personal expertise and preference of the surgeon. The outcome for a specific new patient can only be extrapolated based on experience.

A decision support system (DSS) may provide a second opinion and a more objective basis for the choice of therapy. For mitral valve interventions, a DSS may include modules for reconstructing and simulating the mitral valve as well as the blood flow through the valve under normal or under altered conditions. Such a simulation system should be able to reproduce pathologies, such as prolapse, or take different levels of physical activity of the patient into account. In addition, such a system should provide interactive modules for the exploration of different intervention alternatives and thus provide a visualization of the current anatomy behavior including the different options for modifying the current state. The alternatives could then be safely explored in-silico. After a thorough analysis of the outcome, the results of the simulation after a virtual intervention could provide new insights into the modified dynamics and then influence the therapy decision.

Building and simulating a model that includes all details of the physiology and precisely reproduces the complex dynamics of the left heart including the mitral valve has not yet been realized. Even if all the necessary parameters and a reliable approximation of the in-vivo geometry were available, using today's methods, it can be safely assumed that such a simulation would require many days or even weeks of computation time for one data set. While such an approach is certainly of huge value for biomedical research and education, the system would be more or less useless in a clinical scenario where time is one of the constraints. Therefore, in a DSS scenario, evaluating the model should be fast enough to be used on normal workstations found in a clinical setting.

Our approach addresses the open problem of how simple or complex a MV model has to be in order to be of help in a decision support scenario. As a first step towards a simulation of the MV and its interaction with the LH, we propose a simplified mitral valve and blood flow model. For the first time, we use position-based modeling for the simulation of the MV. Position-based dynamics (PBD) is a fast and stable simulation method that is commonly used in real-time computer graphics and games [MHHR07, BMO*14, MMC16, BMM17]. The models are efficient to evaluate and can be extended later on. In contrast to other approaches, simulations execute at interactive frame rates and can be combined with real-time visualizations. Besides fast computation, accuracy is of central importance. The simulated closed valve state should match the closed state seen in the images and, if present, pathologies should be reproduced. The simulation model should also be able to represent virtual interventions such as annuloplasty, papillary muscle relocation, cord manipulation, and clipping. The novel approach presented here comprises all the mentioned aspects. In addition, we propose a heuristic to approximate the chordae tendineae. Regarding the uncertainties involved, our method achieves a similar quality compared with more complex approaches.

2. Related work

In this section, we briefly review the state of the art concerned with the simulation of the mitral valve behavior. For a more in depth review the reader is referred to Gao et al. [GQF*17]. We limit the review to material models as well as simulation methods and skip imaging, segmentation, and reconstruction techniques that are essential for defining the geometry of the valve. Information on these topics can be found, e.g., in Tautz et al. [TNH*18].

2.1. Material Models and Parameterization

Most groups dealing with modeling the MV use solid mechanics models to represent the material of the valve. This mainly includes the well-known family of (hyper-)elastic material models [MV06]. These models sometimes include the description of fiber directions, which leads to transversely isotropic or anisotropic material models [GOH06, VCV*07, PSH07, VCV*08, PSSH10, DKS18]. The parameterization of these models is challenging and is usually done using autopsy material from human subjects or material obtained from animal experiments. Prot et al. [PSSH10] performed a series of elastic measurements of the human mitral valve. The complexity of the applied fluid mechanics models for blood can vary. Some groups use non-Newtonian fluid models such as the Carreau-Yasuda model [VBG*18]. For a decision support scenario, the mechanical properties of the valve cannot be easily and reliably measured in-vivo, e.g. with regard to calcification or exact fiber directions. The same is true for boundary conditions of the surrounding blood as well as the interaction between fluid and valve. While blood flow velocities can be measured to a certain extent at a specific point in time, changing valvular and hemodynamics in different personal conditions caused, e.g., by drugs, stress or physical exercise cannot be predicted from one measurement alone. The range of possible parameter values is simply too large. While general material properties are known from literature, patient specific peculiarities are not.

Modeling the chordae tendineae is an integral part and is discussed in literature as well. Almost all publications cited above use some sort of cord model. Prot et al. [PSSH10] have conducted a series of mechanical measurements for parameterizing individual cords from different areas of the valve. Drach et al. [DKS18] have performed a high resolution micro computed tomography (μ-CT) scan of a mitral valve specimen. They reconstructed the geometry of the valve as well as the placement of the tendinous cords with regard to the papillary muscle. Afterwards, they evaluated the original as well as the simplified cord distributions and simulated the influence of the configurations on material stresses with Finite Element methods (FEM). A similar work has been conducted by Feng et al. [FQG*18]. Their results indicate that an exact reconstruction of the cord distribution may not be necessary from a macroscopic point of view. Based on their work, it can be assumed that it is sufficient to simplify the cord tree in a simulation of the MV. This has practical implications for patient specific modeling in DSS. While the tips of the papillary muscles can often be more or less easily identified in image data, the tendinous cords that connect the papillary muscles to the leaflets are so minuscule that they can only hardly be seen in most image data. There is no choice other than a manual or heuristic definition of the cords.

2.2. Simulation Approaches

Existing approaches for MV simulation can be categorized in basically three sets. The first category uses a structural mechanics approach and simulates deformation as well as material stresses under load with the Finite Element method [VCV*07, PSH07, VCV*08, PSSH10, BMS12]. The simulation usually begins with the open state valve and aims at reproducing the closure. Closure is achieved, e.g., by applying a pressure force [PSH07]. Image-focused approaches, on the other hand, use registration and morphing [DKS18] or tracking approaches in connection with a material model to achieve closure. Grbić et al. proposed an image-based tracking approach evaluated with ovine hearts based on the semi-automatic definition of an open-state valve and a Finite Element model including chordae distribution [GEM*17]. Burlina et al. suggested to start from an open valve surface and track the leaflets to the closed state. Starting from manual initialization, image-based active contours and an FE model with specific material properties mimic the valve dynamics [BSD*10]. The FE model incorporating the effect of the chordae proposed by Burlina et al. requires mechanical and anatomical information not easily extracted from the image data. They also report only limited validation data [BSD*10]. Another approach by Tautz et al. [TWG*19] combines image-based forces determined via gradient vector flow (GVF) field and position-based dynamics to deform and track the valve from open to closed state. The method is efficient, does not rely on modeling the chordae, and uses only basic material modeling.

The second category has a different focus and uses a single fixed mitral valve state of a specific heart phase for simulating blood flow through the valve [VBG*18, FQG*18]. The simulation methods applied are mostly Finite Volume- or Finite Element-based. The resulting pressure distribution, flow rates, velocity vector fields or flow jets are than further investigated.

The third category combines both aspects in a fluid structure interaction (FSI) simulation [EKR*05, KEC07, CMM*18]. The simulations in the third category are by far the most challenging using today's methods. In general, classical FSI using an Arbitrary Lagrangian Eulerian (ALE) approach has special demands with regard to mesh adaptation or remeshing, especially when dealing with large deformations. Other approaches use immersed boundary techniques [GFQ*17] or approximate the fluid behavior with methods like smoothed particle hydrodynamics (SPH) [CMM*18]. Nevertheless, despite model simplifications, running times for fluid structure interaction simulations are in the order of days or weeks on current hardware [CMM*18]. Running times like these are not practical in a DSS. Numerous publications deal with modeling virtual interventions such as annuloplasty [SMC*11, AEK*12, CRMK14, KPM*18, NTH*19] or clipping [MVG*12]. However, no publication combines all aspects.

3. Material and Methods

The goal of this work is to build a model of the mitral valve and provide an efficient method to evolve the reconstructed MV from the open state to the closed state and back, optionally modeling virtual interventions. To be applicable in a time constrained clinical scenario, certain simplifications have to be made regarding the complexity of the mitral valve apparatus. For the use in a decision support software, we propose a simplified model for the mitral valve in combination with a fast simulation method. The approach is relying on basic material assumptions for the valve and is suitable to virtually represent a set of interventions typically performed to treat mitral valve disease. This strategy avoids explicit modeling of complex mechanical properties associated with either healthy or pathological valves. As stated above, the mechanical properties of

the valve cannot be easily and reliably measured in-vivo. The same is true for exact boundary conditions of the surrounding blood. In our approach, the dynamics is driven by a minimal set of external fluid forces representing the surrounding blood. Under the circumstances explained above, the method's outcome should evaluate good enough to be valuable in a DSS scenario. It should also include ways for future extensions that trade simulation time and precision to address certain shortcomings of the current model.

3.1. Initialization of the Mitral Valve Mesh

The geometry of the MV is reconstructed by the segmentation of the open-state valve in one volume of an image series. Open states can most likely be identified and reconstructed correctly. Here, the patient-specific mitral valves are constructed using the approach published by Tautz et al. [TNH*18]. The open-state valve geometry at time $t_0 = 0$ and the per-phase annulus positions at time frames t_i, $i \geq 0$ are semi-automatically defined on an image series. Assuming that the mitral valve is in its open state at time t_0, the initial triangle mesh $\mathcal{M}(t_0)$ consists of a set of vertices $\mathcal{V}_i$, edges, $\mathcal{E}_{ij}$ and triangles $\mathcal{T}_{ijk}$:

$$\mathcal{V}_i, \quad i = 0,\dots,N, \tag{1}$$
$$\mathcal{E}_{ij} = (\mathcal{V}_i, \mathcal{V}_j),\ i,j \in \{0,\dots,N\},\ i \neq j, \tag{2}$$
$$\mathcal{T}_{ijk} = (\mathcal{V}_i, \mathcal{V}_j, \mathcal{V}_k),\ i,j,k \in \{0,\dots,N\},\ i \neq j \neq k. \tag{3}$$

The initial mesh serves as a basis for the dynamics simulation.

3.2. Simulation of the Dynamics

To model the evolution of the mitral valve over time from open state $\mathcal{M}(t_n)$ to closed state $\mathcal{M}(t_{n+1})$ and back to open state $\mathcal{M}(t_{n+2})$, we only use simple material assumptions and a basic fluid approximation. The model is expressed using the extended position-based dynamics (XPBD) variant described in [MMC16, BMM17]. The vertices $\mathcal{V}_i$ of $\mathcal{M}(t)$ are associated with a mass m_i, a position $\vec{x}_i(t)$, a temporary position $\vec{p}_i(t)$, and a velocity $\vec{v}_i(t)$. The inward-facing normal $\vec{n}_i(t)$ at $\mathcal{V}_i$ is defined using the area-weighted average of the normals of the incident triangles. The normals of the triangles $\mathcal{T}_{ijk}$ are defined as

$$\vec{n}_{ijk}(t) = \frac{(\vec{p}_j(t) - \vec{p}_i(t)) \times (\vec{p}_k(t) - \vec{p}_i(t))}{|(\vec{p}_j(t) - \vec{p}_i(t)) \times (\vec{p}_k(t) - \vec{p}_i(t))|}. \tag{4}$$

For edges $\mathcal{E}_{ij}$, a normalized direction vector

$$\vec{n}_{ij}(t) = \frac{\vec{p}_j(t) - \vec{p}_i(t)}{|\vec{p}_j(t) - \vec{p}_i(t)|} \tag{5}$$

is defined.

To drive the dynamics of the system, a set of external forces

$$\vec{f}_l(\vec{x}_i, t),\ i = 0,\dots,N,\ l = 0,\dots,L \tag{6}$$

and a set of constraints

$$C_m(\vec{p}_0(t),\dots,\vec{p}_N(t)),\ m = 0,\dots,M \tag{7}$$

are used. The forces act on the vertex positions $\vec{x}_i(t)$ whereas the constraints are calculated based on the temporary positions $\vec{p}_i(t)$. The constraints $C_m(\vec{p}_0(t),\dots,\vec{p}_N(t))$ restrict certain movements of the mesh $\mathcal{M}(t)$. More details regarding the usage and definition of the constraints can be found in [MHHR07, BMO*14, MMC16, BMM17].

A two-step Verlet-like approach is used for time-integration. In a first step, the velocities

$$\vec{v}_i(t + \frac{1}{2}\Delta t) = \vec{v}_i(t) + \frac{\Delta t}{m_i} \sum_{l=0}^{L} \vec{f}_l(\vec{x}_i, t) \tag{8}$$

are integrated $\forall i$ based on the external forces $\vec{f}_l(\vec{x}_i, t)$ with time step Δt. Subsequently, the unconstrained positions $\vec{x}_i(t)$ are integrated based on the velocities $\vec{v}_i(t + \frac{1}{2}\Delta t)$ defining the temporary positions

$$\vec{p}_i(t + \frac{1}{2}\Delta t) = \vec{x}_i(t) + \Delta t\, \vec{v}_i(t + \frac{1}{2}\Delta t). \tag{9}$$

A non-linear Gauss-Seidel-type solver is used to iteratively satisfy the constraints $C_m(\vec{p}_0(t),\dots,\vec{p}_N(t))$ (weighted with parameters k_m and compliance parameters α_m, see below) while adjusting the temporary positions $\vec{p}_i(t + \frac{1}{2}\Delta t)$ only. Afterwards, the velocities

$$\vec{v}_i(t + \Delta t) = \frac{\vec{p}_i(t + \frac{1}{2}\Delta t) - \vec{x}_i(t)}{\Delta t} \tag{10}$$

and the positions

$$\vec{x}_i(t + \Delta t) = \vec{p}_i(t + \frac{1}{2}\Delta t) \tag{11}$$

are finally updated in the second Verlet-like step. Time-integration is done until convergence. The number of iterations of the inner Gauss-Seidel loop can be set by the user. A single iteration of the simulation consists of one complete time-integration step and the inner loop.

3.3. Modeling the Material of the Mitral Valve

The mechanical properties of the valve material are approximated as follows. The main idea is that the area of the leaflets has to be conserved while stretching or bending of the leaflets should be minimized. Contact has to be handled as well. To achieve this behavior, we define the material model using four different types of constraints. First, we define stretching constraints

$$C_0(\vec{p}_i(t), \vec{p}_j(t)) = |\vec{p}_j(t) - \vec{p}_i(t)| - l_0 = 0,\ i \neq j \tag{12}$$

for each edge $\mathcal{E}_{ij}$ that limit movements in the direction $\vec{n}_{ij}(t)$ based on the initial length $l_0 = |\vec{p}_j(t_0) - \vec{p}_i(t_0)|$ of the edge $\mathcal{E}_{ij}$ at time $t_0 = 0$. Second, we use bending constraints

$$C_1(\vec{p}_i(t), \vec{p}_j(t), \vec{p}_k(t), \vec{p}_l(t)) = \arccos(\vec{n}_{ijk}(t) \cdot \vec{n}_{ijl}(t)) - \phi_0 = 0,\ k \neq l \tag{13}$$

that limit the dihedral angle $\phi = \arccos(\vec{n}_{ijk}(t) \cdot \vec{n}_{ijl}(t))$ between the normals $\vec{n}_{ijk}(t)$ and $\vec{n}_{ijl}(t)$ of the two neighboring triangles $\mathcal{T}_{ijk}$ and $\mathcal{T}_{ijl}$ either to the initial dihedral angle $\phi_0 = \arccos(\vec{n}_{ijk}(t_0) \cdot \vec{n}_{ijl}(t_0))$ or to $\phi_0 = 0$. Third, we apply area conservation constraints

$$C_2(\vec{p}_i(t), \vec{p}_j(t), \vec{p}_k(t)) = |(\vec{p}_j(t) - \vec{p}_i(t)) \times (\vec{p}_k(t) - \vec{p}_i(t))|^2 - a_0 = 0 \tag{14}$$

for each triangle $\mathcal{T}_{ijk}$ that preserve the triangle area compared to the initial state $a_0 = |(\vec{p}_j(t_0) - \vec{p}_i(t_0)) \times (\vec{p}_k(t_0) - \vec{p}_i(t_0))|^2$. The associated parameters for the three constraint types are k_0, k_1, and k_2 with $k_i \in [0,1]$. In addition, we have to set the compliance parameters $\alpha_{\{0,1,2\}} \in [0,1]$ used in XPBD.

To model contact in the coaptation zone, we define collision constraints $C_3(\vec{p}_i(t),\vec{p}_j(t),\vec{p}_k(t),\vec{p}_l(t)) \geq 0$, $i \neq j \neq k \neq l$ with an AABB-type collision detection, ray-triangle intersection tests [MT97], and a collision response modifying the temporary positions $\vec{p}_{\{i,j,k,l\}}$ in their respective opposite directions to resolve the collision, i.e. $\vec{n}_i(t)$ for $\mathcal{V}_i$ and $\vec{n}_{jkl}(t)$ for $\mathcal{T}_{jkl}$. The distance h is used to determine if a collision with vertex $\mathcal{V}_i$ has occurred on either side of the triangle $\mathcal{T}_{jkl}$ or not. The valve thickness is assumed to be $2h$. The constraint parameters are $k_3 = 1$ and $\alpha_3 = 0$. More details on the self collision constraint can be found in [MHHR07, MMC16].

3.4. Dirichlet Boundary Conditions

Annulus and papillary muscle positions for all phases of the series are included in our model. To reflect the fixed position of the annulus, the annulus vertex positions are added as Dirichlet boundary conditions on the evolution, i.e. for all indices i that belong to an annulus vertex $\mathcal{V}_i^{MA}$, we set $\vec{x}_i(t) = \mathcal{I}(t,\vec{x}_i(t_n),\vec{x}_i(t_{n+1}))$. $\mathcal{I}$ represents an interpolation method that interpolates vertex positions between two annuli at t_n and t_{n+1} at time $t_n \leq t \leq t_{n+1}$. The mass of these annulus vertices $\mathcal{V}_i^{MA}$ is set to $m_i = \infty$. In addition, $\vec{v}_i(t_n) = 0$ for all indices i that belong to the annulus. The papillary muscles are simply approximated by their tip positions and are represented by additional vertices $\mathcal{V}_i^{PM}$. Similar to the annulus, the positions serve as Dirichlet boundary conditions and are interpolated between states t_n and t_{n+1}.

3.5. Tendinous Cords

To complete the MV model, a definition of the tendinous cords for the open state is needed. Following the previous results [DKS18, FQG*18], we simplify and approximate the whole chordae tree by a set of additional edges $\mathcal{E}_{ij}^{CT}$ between either manually or heuristically defined papillary muscles $\mathcal{V}_i^{PM}$ and manually defined leaflet vertices $\mathcal{V}_j$ (cf. Fig. 2). The cord edges can be differentiated in primary and secondary depending on the position of the leaflet vertex. Edges close to the orifice are labeled primary, edges on the body of the leaflet are labeled secondary. For each such edge, we add an additional distance constraint $C_0^{CT}(\vec{p}_i(t),\vec{p}_j(t))$ with different values for the parameter

$$k_0^{CT} = \begin{cases} 0, & |\vec{p}_j(t) - \vec{p}_i(t)| - l_0 < 0 \text{ (compression)}, \\ 1, & |\vec{p}_j(t) - \vec{p}_i(t)| - l_0 > 0 \text{ (stretching)} \end{cases} \tag{15}$$

in the two cases where the edge is compressed or stretched. In this case, $\alpha_0^{CT} = 0$. Using this parameterization, the tendinous cords cannot be stretched longer than their initial lengths l_0. When not under load, they can move freely.

In case the papillary muscles cannot be reliably determined in the image data, we propose a heuristic to define the simplified tendinous cords (cf. Fig. 2). As a first step, the user defines vertices $\mathcal{V}_j$ on the valve that correspond to the primary and secondary cords. As a second step, we fit a plane to the annulus. The normal $\vec{n}^{AP}$ of the annulus plane (AP) doubles as a principal flow direction vector (cf. equation 18). Using the position information of the leaflet vertices and the annulus plane, we define the model cords. We assume just two papillary muscle tips $\mathcal{V}_{\{0,1\}}^{PM}$ (posteromedial and anterolateral) in the following. The set of user defined leaflet vertices is divided into two subsets connecting roughly half of the vertices of the anterior and posterior leaflet (lighter colored vertices in Fig. 2) to one PM tip and the other half (darker colored vertices in Fig. 2) to the other tip. Light and dark are used for indicating the PM tip in Fig. 2, while red and blue are used for distinguishing between anterior and posterior leaflets. The centers of gravity $\vec{c}_{\{0,1\}}$ of both subsets of leaflet vertices connected to each of the two tips are calculated. Using this information, the distances $d_{\{0,1\}}$ of $\vec{c}_{\{0,1\}}$ to the AP are determined. The final tip positions for $\mathcal{V}_{\{0,1\}}^{PM}$ are assumed to be $\vec{c}_{\{0,1\}}^{PM} = \vec{c}_{\{0,1\}} + d_{\{0,1\}} \cdot \vec{n}^{AP}$. Finally, the initial lengths needed for defining each individual cord are set to the sum of two absolute differences: One difference determines the distance of the user defined leaflet vertex to the AP, while the other difference determines the distance of the user defined leaflet vertex to either $\vec{c}_{\{0,1\}}^{PM}$, depending on the cord to be defined. The resulting lengths can be scaled by the user as well.

3.6. Modeling the Fluid

In our model, the surrounding blood is not explicitly modeled, because fluid structure interaction (FSI) typically leads to huge computation times. To approximate the behavior of the surrounding fluid and, coupled to that, the behavior of the mitral valve, we use a set of different and easy to evaluate external force fields. The main flow features are the flow direction vectors $w(\vec{x},t)$ as well as the pressure differences $p(\vec{x},t)$ between ventricle and atrium. We define

$$\vec{f}_0(\vec{x}_i,t) = \vec{w}(\vec{x}_i,t), \tag{16}$$

$$\vec{f}_1(\vec{x}_i,t) = (\vec{w}(\vec{x}_i,t) \cdot \vec{n}_i(t)) \cdot \vec{n}_i(t). \tag{17}$$

The first force field $\vec{f}_0$ pushes the vertices $\mathcal{V}_i$ in the direction $\vec{w}(\vec{x}_i,t)$ of the flow field, while the second force field $\vec{f}_1$ moves the vertices $\mathcal{V}_i$ depending on the similarity of the normal direction $\vec{n}_i(t)$ and the flow vector $\vec{w}(\vec{x}_i,t)$ at position $\vec{x}_i(t)$. The flow vectors are defined as

$$\vec{w}(\vec{x}_i,t) = \begin{cases} w \cdot \vec{n}^{AP}, & \text{(systole)}, \\ -w \cdot \vec{n}^{AP}, & \text{(diastole)} \end{cases} \tag{18}$$

with w being a user defined value that determines the magnitude of the flow. This is the most basic form of a flow field. It is represented by a principal direction vector that changes its sign depending on the heart phase. A pressure force

$$\vec{f}_2(\vec{x}_i,t) = p(\vec{x}_i,t) \cdot \vec{n}_i(t) \tag{19}$$

with pressure difference $p(\vec{x}_i,t) = \pm p$ is applied in normal direction $\vec{n}_i(t)$. p is set by the user and the sign changes depending on the current phase.

The simulation parameters themselves are dimensionless, with the exception of distance that is measured in [mm]. A connection to real time can be established via a scaling factor t_{scale}. This scaling factor is calculated based on the frame times of the image series as well as the number of frames between open and closed state of the anatomy.

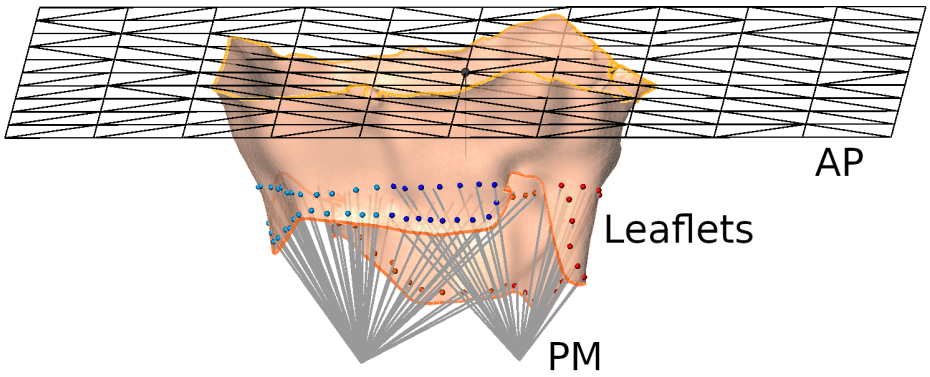

Figure 2: *Setup for defining the chordae tendineae. The papillary muscle tips $\mathcal{V}_i^{PM}$ are marked with **PM** and are connected to the leaflet vertices $\mathcal{V}_j$ via edge $\mathcal{E}_{ij}^{CT}$ (gray lines). In this case, light blue and light red colored vertices connect to one PM tip, while the darker blue and darker red colored vertices are connected to the other PM tip. The annulus plane (**AP**) is shown triangulated and in wire-frame mode. The AP is used for initial length determination of all $\mathcal{E}_{ij}^{CT}$ (see text).*

3.7. Left Heart

In cases where a mesh representation of the left heart is available, it can be included in the simulation. For consistency, it should at least follow the annulus movement (Dirichlet boundary condition), but it should not take part in the integration of the forces. The inclusion of the left heart might be useful for visualization purposes or checks for collisions between leaflets and wall of the heart.

3.8. Virtual Interventions

Using the methods described above, we are able to parameterize the model based on the images series and perform simulations that match the anatomy seen in the images. The parameterized model consisting of the material, forces, and chordae is the basis for the virtual intervention steps. The set of modeled interventions presented here comprises annuloplasty [SMC*11, AEK*12, CRMK14, KPM*18, NTH*19] and the placement of clips [MVG*12], but other scenarios such as cord manipulation or papillary muscle relocation are possible as well. The annuloplasty constrains the shape of the annulus to the chosen annuloplasty ring, which can be represented by a new Dirichlet boundary condition for the annulus. Papillary muscle tips are described by Dirichlet boundary conditions as well. In case of a cord manipulation, cords can be added or removed as well as elongated or shortened by changing the rest length of the edge. Clips can be placed by adding additional edges and additional distance constraints between the vertices of anterior and posterior leaflets. The distance constraints are parameterized like the ones for the tendinous cords but with zero initial length.

4. Results

We applied the method described in Section 3 in two scenarios. At first, we applied the methods to ten reconstructed mitral valves, determined one parameter set for all cases, simulated closure, and compared cross sections visually to their respective TEE image sequences. Second, the parameterized models were used for the simulation of virtual interventions. Annuloplasty and clipping were performed for one data set. The cases were processed and the simulations were performed using a prototypical implementation based on the MeVisLab platform [RBH*11]. This implementation included all methods needed for setting up the simulation.

4.1. Parameterization and Image-based Comparison

The valves were defined based on TEE image sequences, five of which (cases A1-5) were acquired from patients with normal mitral valves, while the remaining five (cases B1-5) were acquired pre-operatively from patients with MR. All images were acquired using a GE Vivid E9 system (GE Healthcare, Chicago, IL, USA). The spatial resolution in planes perpendicular to the acquisition direction ranged from 0.857 to 1.305mm, and the resolution along the acquisition direction ranged from 0.591 to 0.9mm. The frame time (duration between frames) was in the range from 24.2 to 49.4ms (no frame delay), and the number of time frames per sequence ranged from 21 to 43. The number of frames from open to closed state ranged from 3 to 9. This equals 114.8 to 228.6ms (A1-5 114.8 to 228.6ms, B1-5 139.6 to 203.2ms).

Domain experts used the approach from Tautz et al. [TNH*18] to define valve surfaces in one volume per image sequence that shows the valve in the open state. Annulus positions were marked in all phases between the open and the closed state. For the definition of the cords, the leaflet vertices were manually placed, and the heuristic was used for determining the papillary muscle tips, setting up the edge distance constraints and initial lengths.

The simulations were performed using the parameters given in Table 1. We tried to find a single common basis parameterization for all cases. The reasoning behind this was that normal in-vivo pressure differences are quite similar across healthy persons at rest. The same argumentation holds for MV material parameters of healthy subjects. The parametrization itself was experimentally found and suited most data sets in a way that closure was achieved, but no excessive leaflet billowing was observed, matching physiological expectations. More inner loops were required to achieve a

correct collision resolution at times where the external forces were too large, but in the cases presented and with the forces used here, three iterations of the inner loop were sufficient. Each simulation was run until convergence. The simulation time per case was in the order of minutes (longest $<$ 2min (3 Gauss-Seidel iterations/step) and $<$ 5min (20 Gauss-Seidel iterations/step) for case B5) and was dominated by the manual work step in the definition of the valve, cords, and annuli. Further details on the simulation input data and the surface meshes can be found in Table 2. The interactive frame rates that could be achieved with the prototypical implementation on a higher end notebook equipped with current mobile workstation hardware ranged from 40 to 47 frames per second using three inner Gauss-Seidel loops and dropped down to 14 frames per second with 20 inner loops. The duration of the simulated closure ranged from 3.54 to 18.94Δt in simulated time. The scaling factor t_{scale} ranged from 9.4 to 50.8Δt ms. For the healthy cases (A1-5), the scaling factor ranged from 21.8 to 50.8Δt ms, while for the MR cases (B1-5), the scaling factor ranged from 9.4 to 24Δt ms. The total leaflet area was conserved during deformation with just 3 Gauss-Seidel iterations. The largest difference in the valve surface areas before and after deformation was $\approx 4\text{mm}^2$. For most cases, the difference was less than 2mm^2.

We compared the results of the converged simulation with the images of the series that depicted the closed valve. With the chosen parameterization, closure was achieved in all cases. Although we have done no detailed quantitative analysis of the deviations yet, looking at the image scales and using the measurement tools provided by MeVisLab, the deviations were no larger than $\pm$5mm. Instead, we classified the results by ranking them in three quality levels: a simulation result was ranked as *satisfactory* if the closure as well as possible pathologies were reproduced, and the simulated outcome resembled the anatomy seen in the images; *passable* if the closure was reproduced, but there were local deviations from the anatomy seen in the images and the pathologies; or *unsatisfactory* if the valve closure was reproduced, but the deviations of the leaflets were comparatively large (read about $\pm$5mm), and the pathologies were not reproduced. Using this scheme, 3 of the processed cases were ranked as satisfactory, 3 as passable, and 4 as unsatisfactory. Representative results for each quality level are shown in Figs. 3 - 5. The experts stated that the leaflet surfaces generally exhibited folding patterns comparable to the ones observed in in-vivo valves (see Fig. 6). Prolapse was reproduced in cases B3 and B4 (see Fig. 6).

4.2. Virtual Interventions

This section briefly show-cases the virtual interventions that were performed with the proposed methods. In figure 7, images of a simulation of an open valve and a closed valve with ring annuloplasty are shown. The altered left heart geometry was generated with the purely geometric approach by Neugebauer et al. [NTH*19] using a CT scanned ring shape. The left heart mesh was included in the MV simulation. Notice the bulging in the open valve introduced due to the ring annuloplasty. The former incompletely closing valve was closed after the virtual ring annuloplasty. To judge MV stenosis, the geometric orifice area was assessed in the open state. To find an optimal ring size, one could compare different ring sizes and their geometric orifice areas. Figure 8 shows images of a simulation with 1,2 or 3 clips in different positions. The clips could be placed interactively, and the remaining geometric orifice area could be assessed to find an optimal placement.

5. Discussion

The simulation outcome heavily depends on a multitude of aspects, which makes an evaluation rather difficult. At first, there are uncertainties in the manual definitions made by the experts. Part of these uncertainties originate in the image series itself and what was recorded. Temporal and spacial resolution are crucial, especially when imaging rapidly moving leaflets. The simulation has a much higher temporal resolution ($t_{\text{scale}} \in [9.4\Delta t, 50.8\Delta t]$ ms) than the recorded images. That makes it hard to compare the simulated dynamics to single individual images. A comparison would involve some temporal averaging. Other aspects are based on the subjective nature of manual annotations and segmentations of the anatomy. Second, the boundary conditions at the time of image acquisition are usually unknown. Simulation results can only be compared to one example, and, again, comparisons of the complete dynamics are difficult. The superposition of forces in section 3.6 results in time- and position-dependent force fields that change with heart phase and geometry but do not necessarily resemble the exact fluid flow at image acquisition. The same holds for material parameter definitions and cord distributions. In the end, an evaluation judges not just the quality of the model and simulation method used but depends on all of the aspects above. Because of this, we are limiting the discussion here mostly to two aspects: how well is the closure of the valve and how well is the pathology reproduced by our approach. The latter is an even harder task than the former.

Closure can be achieved for all cases. The deviations are similar to other results found in literature for Finite Element models [BMS12]. In the pathological cases, for instance looking at case B3 in Fig. 3, a slight rotation of the closed state annulus would have led to an even better match to the image data. The prolapse is reproduced. In case B5 (shown in Fig. 4), the general shape of the simulated closed valve matches the form seen in the image data, but the result shows a false coaptation zone as well as a different position of the prolapse. This result could either be caused by leaflets of overestimated size or by the assumptions made in the simulation, with regard to cords or forces. The bottom line is that the open-state valve model and the annulus positions have to match the image data well.

An exact cord placement in number and position seems not to be necessary for closure, but lengths as well as length proportions for primary and secondary cords defined by the user are essential for the simulation outcome. Prolapsing valves can be simulated with the heuristic cord setup, but in two of the five cases this was not possible without manual changes in cord setup (cf. Figs. 5).

The simplification of forces is not that critical for closure, but in abnormal cases the current modeling may be too simple. Closure can be reproduced very well, but in case of a prolapse the external forces are sometimes not able to push the leaflets to the recorded end position (e.g. case B2 in Figs. 5), either because of the cord model or because of the collision handling.

Parameter	k_0	k_1	k_2	m	w	p	Δt	$\alpha_{\{0,1,2\}}$	h	It
Value	0.1	0.1	1.0	1.0	± 50.0	± 100.0	0.005	$1e^{-5}$	0.5mm	$\{3, 20\}$

Table 1: *Parameterization for valve simulations used in the evaluation. **It** stands for the number of Gauss-Seidel iterations.*

Case	Vertices	Edges	Faces	Area $[mm^2]$	Time 3 $[ms/\text{It}]$	Time 20 $[ms/\text{It}]$	CD $[ms/\text{It}]$	Conv 3 It	Area 3 $[mm^2]$
A1	1365	3934	2569	1707	19	37	2	772	1706
A2	1643	4759	3116	2076	20	42	3	1052	2073
A3	2252	6547	4293	2780	21	51	4	1636	2784
A4	1491	4311	2820	1860	19	39	2	708	1858
A5	2006	5813	3805	2514	21	47	3	908	2515
B1	2699	7834	5133	3312	22	57	4	1692	3311
B2	2825	8188	5359	3531	22	58	5	1400	3531
B3	2344	6758	4408	2860	21	51	4	1996	2860
B4	1830	5305	3475	2312	20	42	3	800	2310
B5	3008	8778	5770	3855	23	63	5	3788	3855

Table 2: *Case-specific input mesh statistics (left columns), algorithm performance and iterations (It) until convergence (right columns). Cases A refer to normal MVs, cases B to pathological MVs. **Time 3** refers to the time for one complete simulation step with 3 inner Gauss-Seidel loops. Likewise, **Time 20** refers to the time for one simulation step with 20 Gauss-Seidel loops. **CD** stands for the time used for collision detection and **Conv 3** for the number of iterations until convergence (3 inner Gauss-Seidel loops). **Area 3** is given at the time of convergence. The value provides a reference of how well the area constraints preserve the surface area of the valve, in this case with 3 inner Gauss-Seidel loops (compare with values in **Area** column).*

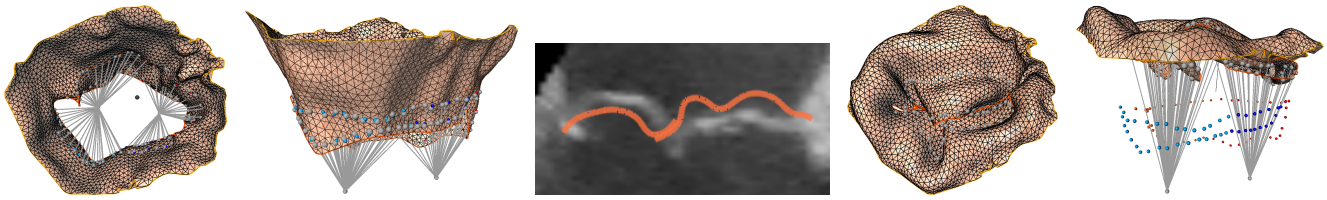

(a) (b) (c) (d) (e)

Figure 3: *Example for a satisfactory simulation (case B3). From left to right: **(a)** Open valve, tendinous cords, and leaflet vertices shown from atrium, **(b)** open valve, **(c)** cross-section of closed valve overlaid on image data, **(d))** closed valve shown from atrium, **(e)** closed valve. The pathology (prolapse) is reproduced in the right location. There is a slight deviation in the leaflet positions (rotation with respect to the AP) because of the annulus placement.*

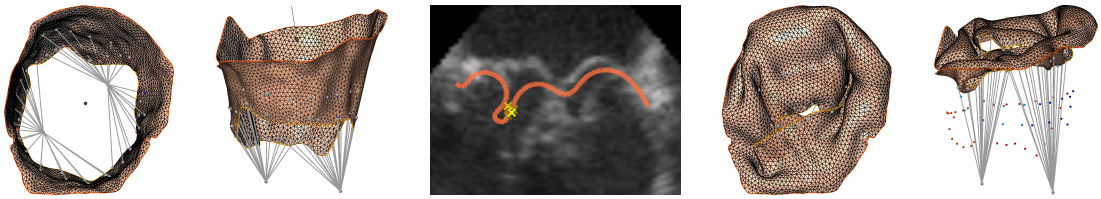

(a) (b) (c) (d) (e)

Figure 4: *Example for a passable simulation (case B5). From left to right: **(a)** Open valve, tendinous cords, and leaflet vertices shown from atrium, **(b)** open valve, **(c)** cross-section of closed valve overlaid on image data, **(d))** closed valve shown from atrium, **(e)** closed valve. The pathology (prolapse) is reproduced but in the wrong position. The coaptation is shifted.*

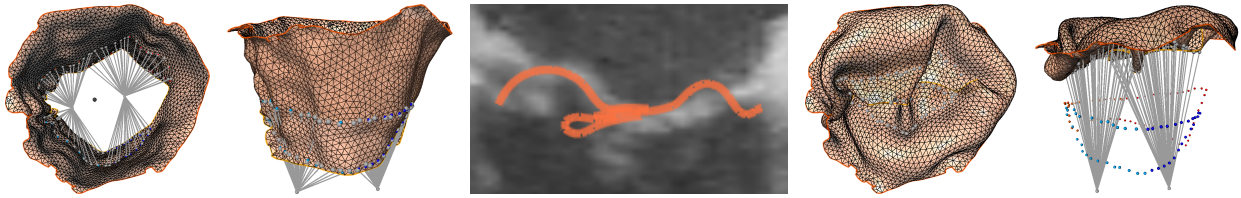

(a) (b) (c) (d) (e)

Figure 5: *Example for a unsatisfactory simulation (case B2). From left to right:* ***(a)*** *Open valve, tendinous cords, and leaflet vertices shown from atrium,* ***(b)*** *open valve,* ***(c)*** *cross-section of closed valve overlaid on image data,* ***(d))*** *closed valve shown from atrium,* ***(e)*** *closed valve. Although the approximation is good, the pathology is not reproduced.*

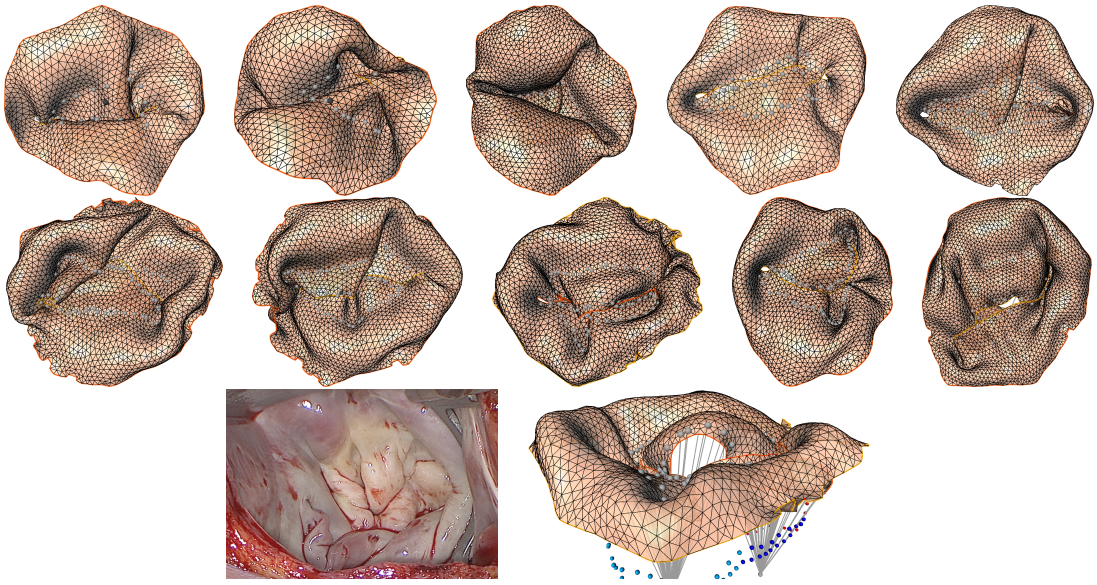

Figure 6: *Visual comparison of a simulated valve closure (top row A1-5, middle row B1-5) and an endoscopic view on a mitral valve during minimal-invasive heart surgery with arrested heart (bottom row, left side, different patient). Note the folding and bulges of the leaflet surface in both the surface models and the in-vivo valve. The shape of the simulated prolapse of case B3 is depicted in the image located in the bottom row, on the right side. The result matches the indication for surgery.*

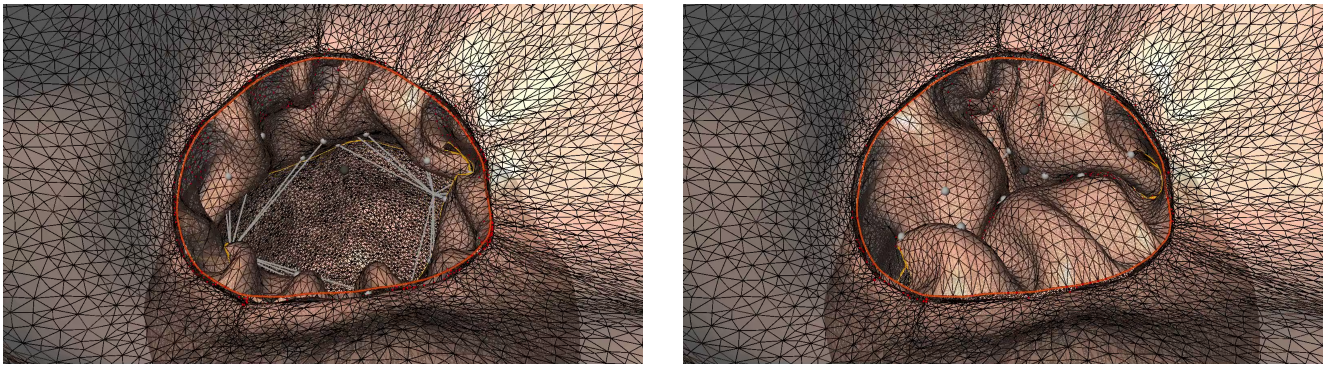

(a) (b)

Figure 7: *Ring annuloplasty:* ***(a)*** *diastolic opening,* ***(b)*** *systolic closure. The surrounding left heart mesh is included in the simulation. The point of view is located in the atrium.*

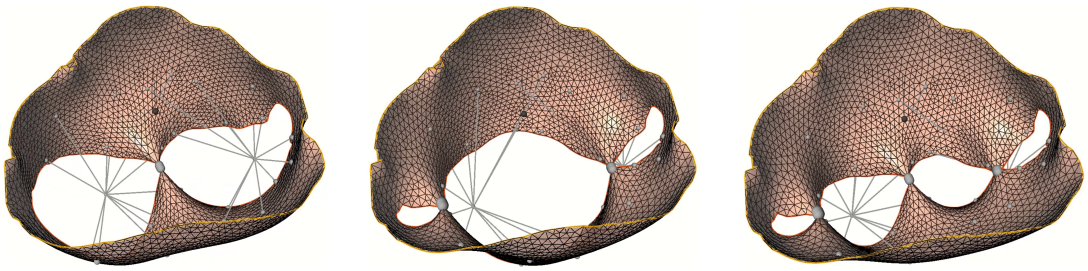

(a) (b) (c)

Figure 8: *Clipping with 1-3 clips. All valves shown at diastole. The geometric orifice area can be assessed.*

6. Conclusion

We presented first results of a fast simulation method for the mitral valve that runs at interactive frame rates and can even be sped up further using a GPU implementation. Regarding the simulation times, we think the chosen ansatz is suitable in a decision support scenario. The approach combines a simple material model expressed in position-based dynamics with a set of external forces that represent the fluid. An initial qualitative evaluation with a limited number of normal and abnormal cases showed that the deformation of our model forms closed valve shapes that resemble real valves in general. The shapes of the simulated closed valves mostly fit to the anatomy depicted in the image series. The absolute deviations are similar to values found in literature. However, there are still local deviations that probably stem from uncertainties in the parameterization, e.g. with regard to unknown local material properties or fluid influences as well as subjective definitions for leaflets, annuli, or tendinous cords. In the future, we plan to do a quantitative evaluation and investigate the aspects that lead to the described shortcomings. A natural extension of the current approach consists of using more sophisticated position-based material models [BMM17] that also describe local variations. For an easier setup, the parameterization of the valve material should be automated, e.g., by adopting an inverse approach such as [Noe18]. To fully answer the question of what cord configuration results in a prolapse, an automated inverse problem solver that can add or subtract and elongate or shorten cords may be beneficial. To complete the model, the movement of the left heart as well as fluid structure interaction should be added to the model. In addition, the results of the virtual interventions have to be validated on post-op image data.

Acknowledgment This work is part of the BMBF VIP+ project DSS Mitral (partially funded by the German Federal Ministry of Education and Research under grant 03VP00852).

References

[AEK*12] AMINI R., ECKERT C. E., KOOMALSINGH K., MCGARVEY J., MINAKAWA M., GORMAN J. H., GORMAN R. C., SACKS M. S.: On the in vivo deformation of the mitral valve anterior leaflet: Effects of annular geometry and referential configuration. *Annals of Biomedical Engineering 40*, 7 (Jul 2012), 1455–1467. doi:10.1007/s10439-012-0524-5. 3, 6

[Bla14] BLAUSEN.COM STAFF: Medical gallery of Blausen Medical 2014. WikiJournal of Medicine 1(2):10, 2014. doi:10.15347/wjm/2014.010. 2

[BML*18] BECKMANN A., MEYER R., LEWANDOWSKI J., FRIE M., MARKEWITZ A., HARRINGER W.: German Heart Surgery Report 2017: The Annual Updated Registry of the German Society for Thoracic and Cardiovascular Surgery. *The Thoracic and Cardiovascular Surgeon 66*, 08 (Nov. 2018), 608–621. doi:10.1055/s-0038-1676131. 1

[BMM17] BENDER J., MÜLLER M., MACKLIN M.: Position-based simulation methods in computer graphics. In *EUROGRAPHICS 2017 Tutorials* (2017), Eurographics Association. doi:10.2312/egt.20171034. 2, 4, 10

[BMO*14] BENDER J., MÜLLER M., OTADUY M. A., TESCHNER M., MACKLIN M.: A survey on position-based simulation methods in computer graphics. *Computer Graphics Forum 33*, 6 (2014), 228–251. doi:10.1111/cgf.12346. 2, 4

[BMS12] BURLINA P., MUKHERJEE R., SPROUSE C.: A personalized mitral valve closure simulator. In *2012 Annual International Conference of the IEEE Engineering in Medicine and Biology Society* (Aug 2012), pp. 6636–6640. doi:10.1109/EMBC.2012.6347516. 3, 7

[BSD*10] BURLINA P., SPROUSE C., DEMENTHON D., JORSTAD A., JUANG R., CONTIJOCH F., ABRAHAM T., YUH D. D., MCVEIGH E. R.: Patient-Specific Modeling and Analysis of the Mitral Valve Using 3D-TEE. In *IPCAI* (2010), Springer, pp. 135–146. 3

[CMM*18] CABALLERO A., MAO W., MCKAY R., PRIMIANO C., HASHIM S., SUN W.: New insights into mitral heart valve prolapse after chordae rupture through fluid–structure interaction computational modeling. *Scientific Reports 8*, 17306 (2018). doi:10.1038/s41598-018-35555-5. 3

[CRMK14] CHOI A., RIM Y., MUN J. S., KIM H.: A novel finite element-based patient-specific mitral valve repair: virtual ring annuloplasty. *Bio-medical materials and engineering 24*, 1 (2014), 341 – 347. URL: https://www.ncbi.nlm.nih.gov/pubmed/24211915. 3, 6

[DKS18] DRACH A., KHALIGHI A. H., SACKS M. S.: A comprehensive pipeline for multi-resolution modeling of the mitral valve: Validation, computational efficiency, and predictive capability. *International Journal for Numerical Methods in Biomedical Engineering 34*, 2 (2018), e2921. e2921 CNM-May-17-0128.R1. doi:10.1002/cnm.2921. 3, 5

[EKR*05] EINSTEIN D. R., KUNZELMAN K. S., REINHALL P. G., NICOSIA M. A., COCHRAN R. P.: Non-linear fluid-coupled computational model of the mitral valve. *The Journal of heart valve disease 14 3* (2005), 376–85. 3

[FQG*18] FENG L., QI N., GAO H., SUN W., VÁZQUEZ M., GRIFFITH B. E., LUO X.: On the chordae structure and dynamic behaviour of the mitral valve. In *IMA journal of applied mathematics* (2018). 3, 5

[GEM*17] GRBIC S., EASLEY T. F., MANSI T., BLOODWORTH C. H.,

PIERCE E. L., VOIGT I., NEUMANN D., KREBS J., YUH D. D., JENSEN M. O., COMANICIU D., YOGANATHAN A. P.: Personalized mitral valve closure computation and uncertainty analysis from 3D echocardiography. *Medical Image Analysis 35* (Jan. 2017), 238–249. doi:10.1016/j.media.2016.03.011. 3

[GFQ*17] GAO H., FENG L., QI N., BERRY C., GRIFFITH B. E., LUO X.: A coupled mitral valve—left ventricle model with fluid–structure interaction. *Medical Engineering & Physics 47* (2017), 128 – 136. doi:10.1016/j.medengphy.2017.06.042. 3

[GOH06] GASSER T., OGDEN R., HOLZAPFEL G.: Hyperelastic modelling of arterial layers with distributed collagen fibre orientations. *Journal of the Royal Society Interface 3*, 6 (2006), 15 – 35. doi:10.1098/rsif.2005.0073. 3

[GQF*17] GAO H., QI N., FENG L., MA X., DANTON M., BERRY C., LUO X.: Modelling mitral valvular dynamics–current trend and future directions. *International Journal for Numerical Methods in Biomedical Engineering 33*, 10 (2017), e2858. e2858 cnm.2858. doi:10.1002/cnm.2858. 2

[KEC07] KUNZELMAN K., EINSTEIN D., COCHRAN R.: Fluid–structure interaction models of the mitral valve: function in normal and pathological states. *Philosophical Transactions of the Royal Society B: Biological Sciences 362*, 1484 (Jun 2007). doi:10.1098/rstb.2007.2123. 3

[KPM*18] KONG F., PHAM T., MARTIN C., ELEFTERIADES J., MCKAY R., PRIMIANO C., SUN W.: Finite element analysis of annuloplasty and papillary muscle relocation on a patient-specific mitral regurgitation model. *PLOS ONE 13*, 6 (06 2018), 1–15. doi:10.1371/journal.pone.0198331. 3, 6

[KSH18] KLAWKI R., SCHMIDT K., HEINEMANN M. (Eds.): *Deutscher Herzbericht 2018*. 2018. 1

[MHHR07] MÜLLER M., HEIDELBERGER B., HENNIX M., RATCLIFF J.: Position based dynamics. *Journal of Visual Communication and Image Representation 18*, 2 (2007), 109 – 118. doi:10.1016/j.jvcir.2007.01.005. 2, 4, 5

[MMC16] MACKLIN M., MÜLLER M., CHENTANEZ N.: XPBD: Position-based Simulation of Compliant Constrained Dynamics. In *Proceedings of the 9th International Conference on Motion in Games* (New York, NY, USA, 2016), MIG '16, ACM, pp. 49–54. doi:10.1145/2994258.2994272. 2, 4, 5

[MT97] MÖLLER T., TRUMBORE B.: Fast, minimum storage ray-triangle intersection. *J. Graph. Tools 2*, 1 (Oct. 1997), 21–28. doi:10.1080/10867651.1997.10487468. 5

[MV06] MARCKMANN G., VERRON E.: Comparison of hyperelastic models for rubber-like materials. 3

[MVG*12] MANSI T., VOIGT I., GEORGESCU B., ZHENG X., MENGUE E. A., HACKL M., IONASEC R. I., NOACK T., SEEBURGER J., COMANICIU D.: An integrated framework for finite-element modeling of mitral valve biomechanics from medical images: Application to mitralclip intervention planning. *Medical Image Analysis 16*, 7 (2012), 1330 – 1346. Special Issue on the 2011 Conference on Medical Image Computing and Computer Assisted Intervention. doi:10.1016/j.media.2012.05.009. 3, 6

[Noe18] NOE U.: *Bayesian nonparametric inference in mechanistic models of complex biological systems*. PhD thesis, University of Glasgow, 2018. URL: http://encore.lib.gla.ac.uk/iii/encore/record/C__Rb3336090. 10

[NTH*19] NEUGEBAUER M., TAUTZ L., HÜLLEBRAND M., SÜNDERMANN S., DEGENER F., GOUBERGRITS L., KÜHNE T., FALK V., HENNEMUTH A.: Virtual downsizing for decision support in mitral valve repair. *International Journal of Computer Assisted Radiology and Surgery 14*, 2 (Feb 2019), 357–371. doi:10.1007/s11548-018-1868-6. 3, 6, 7

[PSH07] PROT V., SKALLERUD B., HOLZAPFEL G. A.: Transversely isotropic membrane shells with application to mitral valve mechanics. constitutive modelling and finite element implementation. *International Journal for Numerical Methods in Engineering 71*, 8 (2007), 987–1008. doi:10.1002/nme.1983. 3

[PSSH10] PROT V., SKALLERUD B., SOMMER G., HOLZAPFEL G.: On modelling and analysis of healthy and pathological human mitral valves: Two case studies. *Journal of the Mechanical Behavior of Biomedical Materials 3*, 2 (2010), 167 – 177. doi:10.1016/j.jmbbm.2009.05.004. 3

[RBH*11] RITTER F., BOSKAMP T., HOMEYER A., LAUE H., SCHWIER M., LINK F., PEITGEN H.: Medical Image Analysis. *IEEE Pulse 2*, 6 (Nov. 2011), 60–70. doi:10.1109/MPUL.2011.942929. 6

[SBF*08] SEEBURGER J., BORGER M. A., FALK V., KUNTZE T., CZESLA M., WALTHER T., DOLL N., MOHR F. W.: Minimal invasive mitral valve repair for mitral regurgitation: results of 1339 consecutive patients. *European Journal of Cardio-Thoracic Surgery 34*, 4 (Oct. 2008), 760–765. doi:10.1016/j.ejcts.2008.05.015. 1

[SMC*11] STEVANELLA M., MAFFESSANTI F., CONTI C. A., VOTTA E., ARNOLDI A., LOMBARDI M., PARODI O., CAIANI E. G., REDAELLI A.: Mitral valve patient-specific finite element modeling from cardiac mri: Application to an annuloplasty procedure. *Cardiovascular Engineering and Technology 2*, 2 (Jun 2011), 66–76. doi:10.1007/s13239-010-0032-4. 3, 6

[SSB*14] SÜNDERMANN S. H., SROMICKI J., BIEFER H. R. C., SEIFERT B., HOLUBEC T., FALK V., JACOBS S.: Mitral valve surgery: Right lateral minithoracotomy or sternotomy? A systematic review and meta-analysis. *The Journal of Thoracic and Cardiovascular Surgery 148*, 5 (2014), 1989 – 1995.e4. doi:10.1016/j.jtcvs.2014.01.046. 1

[TNH*18] TAUTZ L., NEUGEBAUER M., HÜLLEBRAND M., VELLGUTH K., DEGENER F., SÜNDERMANN S., WAMALA I., GOUBERGRITS L., KUEHNE T., FALK V., HENNEMUTH A.: Extraction of open-state mitral valve geometry from CT volumes. *International Journal of Computer Assisted Radiology and Surgery* (Aug. 2018). doi:10.1007/s11548-018-1831-6. 2, 4, 6

[TWG*19] TAUTZ L., WALCZAK L., GEORGII J., JAZAERLI A., VELLGUTH K., WAMALA I., SÜNDERMANN S., FALK V., HENNEMUTH A.: Combining position-based dynamics and gradient vector flow for mitral valve tracking in tee ultrasound, accepted for publication. In *International Journal of Computer Assisted Radiology and Surgery* (2019). 3

[VBG*18] VELLGUTH K., BRÜNING J., GOUBERGRITS L., TAUTZ L., HENNEMUTH A., KERTZSCHER U., DEGENER F., KELM M., SÜNDERMANN S., KUEHNE T.: Development of a modeling pipeline for the prediction of hemodynamic outcome after virtual mitral valve repair using image-based cfd. *International Journal of Computer Assisted Radiology and Surgery 13*, 11 (Nov 2018), 1795–1805. doi:10.1007/s11548-018-1821-8. 3

[VCV*07] VOTTA E., CAIANI E., VERONESI F., SONCINI M., ONTEVECCHI F. M., REDAELLI A.: Finite element modelling of the mitral valve : feasible approaches for understanding the valvular function and evaluating clinical scenarios. 3

[VCV*08] VOTTA E., CAIANI E., VERONESI F., SONCINI M., MONTEVECCHI F. M., REDAELLI A.: Mitral valve finite-element modelling from ultrasound data: a pilot study for a new approach to understand mitral function and clinical scenarios. *Philosophical Transactions of the Royal Society A: Mathematical, Physical and Engineering Sciences 366*, 1879 (Jul 2008). doi:10.1098/rsta.2008.0095. 3